Jurnal Riset Kimia

ISSN (print) : 1978-628X
ISSN (online) : 2476-8960

Structure, Morphology, Optical, Magnetic and Dielectric Properties of $Ni_{1-x}Cd_xFe_2O_4$ Material Synthesized by Autocombustion Method

Poppi Darmila Libra, Syukri, Yeni Stiadi, Rahmayeni*

[1]Department of Chemistry, Faculty of Mathematics and Natural Sciences, Universitas Andalas, Kampus Limau Manis, Padang, Indonesia

Corresponding Author:
Rahmayeni
rahmayenni@sci.unand.ac.id

Received: June 2025
Accepted: September 2025
Published: September 2025

© Rahmayeni et al. This is an open-access article distributed under the terms of the Creative Commons Attribution License, which permits unrestricted use, distribution, and reproduction in any medium, provided the original author and source are credited.

Abstract

Materials with nanoscale dimensions have recently attracted attention due to their outstanding electrical, magnetic, and dielectric capabilities. Electromagnetic materials, known as spinel ferrite MFe_2O_4 (M = divalent ion), are essential in advanced technology. Cadmium-substituted ferrite spinel with composition $Ni_{1-x}Cd_xFe_2O_4$ (x = 0, 0.1, 0.15, and 0.2) was synthesized by the autocombustion method using citric acid as a fuel agent. X-Ray Diffraction (XRD) confirms that the spinel structure is present in the prepared nanocrystalline ferrites. Fourier Transformed Infrared Spectroscopy (FTIR) spectra showed intensive absorption bands in the 400-600 cm^{-1} range corresponding to tetrahedral and octahedral sites. The absorption spectrum of FTIR shifts towards lower wave numbers as the Cd^{2+} ion concentration increases. Cd^{2+} ions doping is important for crystal growth, as evidenced by Scanning Electron Microscopy (SEM) images. The band gap energy values of $Ni_{1-x}Cd_xFe_2O_4$ samples are 1.53 eV, 1.46 eV, 1 43eV, 1.42 eV for x=0-0.2, which indicates the samples absorb in visible light. Analysis of magnetic properties with Vibrating Sample Magnetometer (VSM) shows a small hysteresis loop, so $Ni_{1-x}Cd_xFe_2O_4$ is a soft magnetic material. The dielectric constant increases as the Cd^{2+} ion concentration increases. The characterization outcomes recommend that the compounds can be used for several applications such as memory, and energy storage devices.

Keywords: *$Ni_{1-x}Cd_xFe_2O_4$; autocombustion; structural; magnetic; dielectric.*

Introduction

The development of technology and industry has led to an increase in the need for energy every year, resulting in the increasingly depleted availability of energy sources. Therefore, various efforts have been made to obtain new energy sources. Energy storage is important so that energy can be used optimally. This condition requires researchers to develop a technology to overcome energy problems, especially in energy storage. Nanoscale materials have recently attracted attention because of their extraordinary electrical, magnetic, and dielectric capabilities, so that they can be utilized in energy storage applications[1].

Spinel ferrite compounds have attracted the attention of researchers in recent decades due to their unique properties and potential applications in various fields of science and technology. Spinel ferrite materials with the formula MFe_2O_4 where M is a divalent metal ion such as Ni^{2+}, Co^{2+}, Cu^{2+}, Mn^{2+}, Mg^{2+}, Zn^{2+}, and Fe^{2+} play an important role in energy storage applications because they have high stability, low conductivity and good magnetic properties. Spinel ferrite electromagnetic materials are very

DOI: https://doi.org/ 10.25077/jrk.v16i2.855

important in the field of advanced technology[2]. Spinel ferrite is a functional material that can be used in various applications such as microwave devices, antenna rods, telecommunications, radar, catalysts, sensors and low and high frequency storage devices[3]. The addition of metal or metal oxide dopants into nanoferrite compounds is a common technique used to modify the structure, particle size, and lattice strain that have an impact on various properties including increasing surface area, volume and pore size, active sites, magnetic properties, and electrical properties[4].

One of the magnetic spinel ferrite nanoparticles that is currently widely developed is nickel ferrite nanoparticles ($NiFe_2O_4$)[5]. Nickel ferrite is an important material used in technological applications, humidity sensors, gas sensing, and supercapacitors because it has good catalytic behavior, high chemical stability[6], low conductivity and good magnetic properties[7]. Various modifications have been made to obtain better properties of nickel ferrite, one of which is through doping. Several metal ions have been used for nickel ferrite modification such as Cu^{2+}, Nd^{2+}, Zn^{2+} and Co^{2+} [8]–[11]. The substitution of non-magnetic Cd^{2+} ions in nickel ferrite is considered very useful with wide applications in electronic and microwave devices because it has high electrical resistivity, low eddy current, and dielectric loss.

$CdFe_2O_4$ has a normal spinel structure, and $NiFe_2O_4$ has an inverse spinel structure, since Ni^{2+} strongly prefers octahedral sites. Cadmium is a non-magnetic divalent ion that essentially occupies tetrahedral sites when substituted in ferrite. Substitution of Cd^{2+} ions in ferrite is known to improve its magnetic and electrical properties, such as saturation magnetization[12]. Due to the wide range of uses of this material, much research has been done in the field of cadmium ferrite synthesis. However, additional studies are needed to synthesize high-purity cadmium ferrite with a regular size and morphology[13].

The synthesis method of ferrite nanoparticles greatly affects their composition, structure, and morphology. Various methods have been used to synthesize ferrite nanoparticles, including coprecipitation[14], microemulsion[15], sol-gel autocombustion[16], citric acid precursor, reflux[17], and solid state chemical reactions[18]. Each method has advantages and disadvantages, such as simplicity, ease, temperature, and use of hazardous chemicals[19]. These methods use different synthesis temperatures to produce ferrite nanoparticles with different crystal sizes[2]. The autocombustion method has been used for the synthesis of various materials because it is simpler, and the resulting products have regular morphology, low calcination temperature, smaller nanoparticle size, and large surface area[20].

In this study, the synthesis of $NiFe_2O_4$ spinel ferrite doped with Cd^{2+} ions into $Ni_{1-x}Cd_xFe_2O_4$ was carried out using the autocombustion method with citric acid as fuel. This study investigates the effect of Cd doping on the structural and characteristic properties of $Ni_{1-x}Cd_xFe_2O_4$. The autocombustion method is simpler and friendly for the environment. Sample characterization was carried out with several instruments such as XRD to analyze its structure, SEM-EDS to analyze the surface morphology and composition of spinel ferrite. The magnetic and dielectric properties of the material were analyzed using VSM equipment and the dielectric properties with an LCR meter. Several relaxation peaks were observed at high frequencies, so they can be used for high-frequency device applications[21].

Experimental

Equipment

The tools used in this study are: glassware (iwaki-pyrex), hot plate stirrer, analytical balance (KERN ABJ 220-4NM), furnace (Naberthem Muffle), and magnetic bar. For the purpose of sample analysis, instruments used include: X-Ray Diffraction (XRD) (Philips X'pert Powder PAN Analytical), Fourier Transform Infrared (FTIR) (PerkinElmer Universal ATR sampling Accessory), Ultraviolet-Visible Diffuse

Reflectance Spectroscopy (DRS UV-Vis) (SPECORD 210 PLUS 223F1936C), Scanning Electron Microscopy-Energy Dispersive Spectroscopy (SEM-EDS) (FE Inspect S50), Vibrating Sample Magnetometer (VSM) (VSM-250 Electromagnetic) and (Inductance, Capacitance and Resistance) LCR meter.

Material

The materials used were $Cd(NO_3)_2.4H_2O$ (Aldrich), silver paste (Aldrich), $Ni(NO_3)_2.6H_2O$ (Merck), distilled water, $Fe(NO_3)_3.9H_2O$ (Merck), copper plate, PVA (Aldrich), Pt wire, distillated water, and citric acid (Merck).

Methods

Synthesis $CdFe_2O_4$ and $NiFe_2O_4$

$CdFe_2O_4$ was synthesized according to the following procedure: 8.1 g of $Fe(NO_3)_3.9H_2O$ were dissolved in 100 mL of aquadest and mixed with 3.44 g of $Cd(NO_3)_2.4H_2O$ solution in 100 mL of aquadest. The mixture was stirred and 3.84 g of citric acid were added. The mixture was continuously stirred at 85°C until the autocombustion process was achieved. After that, the sample was ground until smooth and calcined at 600°C for 3 h [22]. Meanwhile, in another place it is being prepared $NiFe_2O_4$ by dissolving 8.1 g of $Fe(NO_3)_3.9H_2O$ in 100 mL of aquadest and mixing with 2.9 g of $Ni(NO_3)_2.6H_2O$ solution in 100 mL of aquadest. The mixture was stirred and then 3.84 g of citric acid were added. Then the mixture was continuously stirred at 85°C until the autocombustion process was achieved. The samples were ground until smooth and calcined at 600°C for 3 h [22]. The resulting $CdFe_2O_4$ and $NiFe_2O_4$ samples were measured with several equipment.

Synthesis $Ni_{1-x}Cd_xFe_2O_4$ by autocombustion method

$Ni_{1-x}Cd_xFe_2O_4$ nanomaterials (x= 0; 0.1; 0.15; and 0.2) were synthesized using the autocombustion method. The synthesis was conducted by dissolving a certain amount of $Fe(NO_3)_3.9H_2O$, $Cd(NO_3)_2.4H_2O$ and $Ni(NO_3)_2.6H_2O$ (x = 0; 0.1; 0.15; and 0.2) that had been calculated stoichiometrically, then citric acid was added with a mole ratio of metal nitrate and citric acid of 1:2[23]. After that, the mixture was stirred using a magnetic stirrer at a temperature of 85 °C at a speed of 600 rpm until the autocombustion process was achieved. Furthermore, the sample was ground until smooth and calcined at a temperature of 600 °C for 3 hours[22] . The resulting $Ni_{1-x}Cd_xFe_2O_4$ sample was analyzed using several equipment.

Dielectric properties determination

The dielectric properties of the samples in pellet form were tested using an LCR meter. The pellets were prepared as follows: A number of $Ni_{1-x}Cd_xFe_2O_4$ was added with 5 wt. %. of PVA using aquabidest as a reaction medium. The mixture of samples and PVA was ground with a mortar and pestle until homogeneous, dried, and converted into a fine powder. The resulting powder was then pressed into pellets using a hydraulic press at a pressure of 6–7 tons. The pellets were subsequently sintered at 950 °C, after which they were coated with silver paste and platinum wires were attached to both surfaces. The prepared samples were analyzed for their complex dielectric properties at frequency variations of 10 kHz - 300 kHz and at temperature variations of 30 – 500℃ [8].

Results and Discussion

The synthesized samples are shown in Figure 1. The $CdFe_2O_4$ sample appears as a brown powder, whereas $NiFe_2O_4$ exhibits a blackish-brown color. This variation in color reflects the differences in the metal ions incorporated. A similar observation was also reported by previous researchers, who synthesized $Ni_{1-x}Zn_xFe_2O_4$ (x = 0.0–1.0) using the sol–gel autocombustion method, yielding powders with colors ranging from brown to blackish-brown[24].

 DOI: https://doi.org/ 10.25077/jrk.v16i2.855

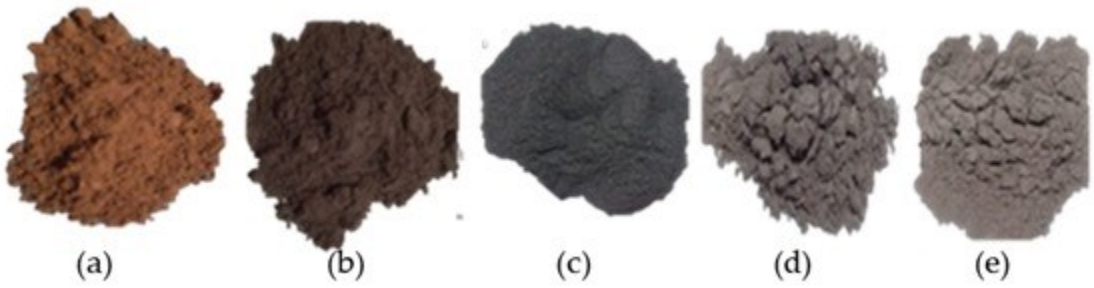

Figure 1. Photo of the synthesized samples of (a) $CdFe_2O_4$, (b) $NiFe_2O_4$, and $Ni_{1-x}Cd_xFe_2O_4$ (x =0.1- 0.2)

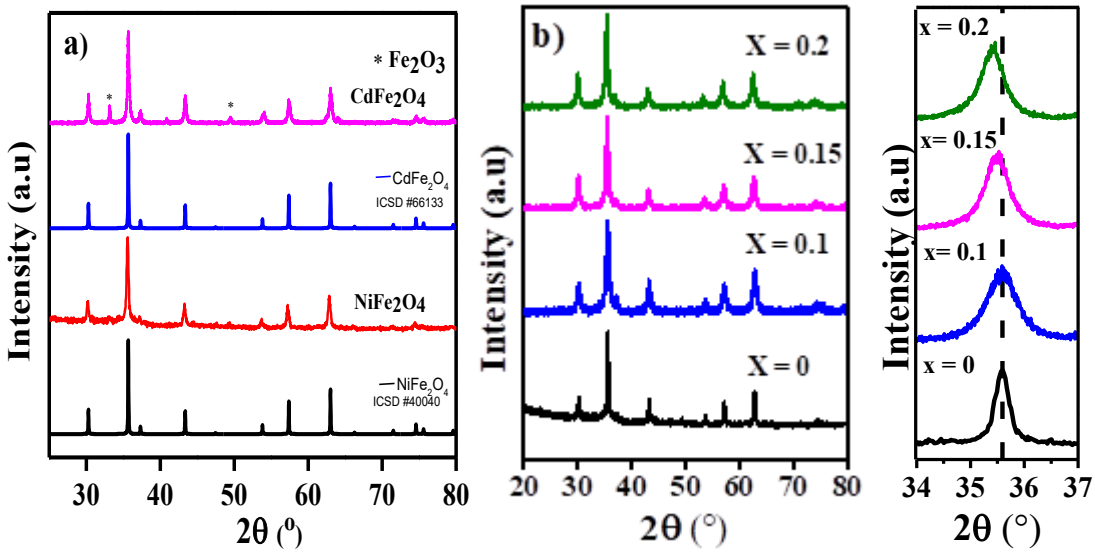

Figure 2. XRD pattern of the sample a) $NiFe_2O_4$ and $CdFe_2O_4$, and b) $Ni_{1-x}Cd_xFe_2O_4$ (x = 0.1-0.2)

$NiFe_2O_4$ appears as a blackish powder, consistent with the results reported by previous researchers. [19]. The resulting $Ni_{1-x}Cd_xFe_2O_4$ is a blackish brown to brown powder. The increasing mass of Cd^{2+}, the color of the resulting $Ni_{1-x}Cd_xFe_2O_4$ ferrite will be increasingly brown. The addition of more Cd^{2+} mass causes the color to change back to brown because Cd^{2+} successfully enters the $Ni_{1-x}Cd_xFe_2O_4$ system[12].

Analysis by XRD

XRD measurements were performed to analyze the structure, crystallinity, and crystal size of the synthesized samples. The obtained data were presented as diffractograms of 2θ versus peak intensity, which were subsequently compared with standard reference data. Figure 2 displays the XRD patterns of the standard, $CdFe_2O_4$, and $NiFe_2O_4$ samples, with the specific peaks of both synthesized samples. The specific peaks of the $NiFe_2O_4$ sample appear at angles 2θ = 30.3°, 35.7°, 37.4°, 43.4°, 53.9°, 57.4°, and 63.1° according to the Miller indexes of (220), (311), (222), (400), (422), (511), and (440), respectively[25], while in the $CdFe_2O_4$ sample peaks appear at angles 2θ = 29.0°, 34.1°, 43.4°, 54.7°, 60.05°, 68.0°, and70.9° with the Miller indices of (220), (311), (422), (511), (440), (620), and (533), respectively[26]. The presence of all these peaks confirms the development of the cubic spinel structure. The diffraction pattern that appears in the $NiFe_2O_4$ sample is in accordance with the ICSD standard #40040. In the $CdFe_2O_4$ sample the diffraction pattern appears in accordance with the ICSD standard #66133. From Figure 2, it can be observed that there are other phases formed in the $CdFe_2O_4$ sample at angles 2θ = 33.2 and 49.2 which are specific peaks of Fe_2O_3 according to the ICSD standard #172906. Data obtained by previous researchers also showed the same impurities from Fe_2O_3.

Figure 2 shows the XRD pattern of $Ni_{1-x}Cd_xFe_2O_4$ samples. The specific peaks appeared at angles of 2θ = 30.25°, 35.7°, 37.25°, 43.3°, 53.75°, 57.25°, and 63° for x = 0.1. Sample x = 0.15 appears peaks 2θ = 30.15°, 35.5°, 37.15°, 43.25°, 53.6°, 57.15°, and 62.75°. At x = 0.2 appeared peaks 2θ = 30.1°, 35.35°, 37°,43.1°, 53.3°, 56.9°, and 62.6° [27] . The specific peak shift was observed around the angle of 35.6° at the position (311) refers to the change in lattice parameters associated with changes in crystallite size of the $Ni_{1-x}Cd_xFe_2O_4$ sample due to the larger radius of the Cd^{2+} doping ion (0.92 Å) than Ni^{2+} (0.72 Å) [12],[28]. The higher the Cd^{2+} concentration in the sample, the more pronounced the shift toward lower 2θ angles, confirming that Cd^{2+} ions successfully occupy the Ni lattice sites[27]. The synthesis results showed no impurity phases originating from αFe_2O_3 or other oxides [29]. The average crystallite size of the synthesized $CdFe_2O_4$, $NiFe_2O_4$ and $Ni_{1-x}Cd_xFe_2O_4$ was calculated using the Debye Scherrer equation[28].

$$L = \frac{K\lambda}{\beta \cos\theta} \quad (1)$$

Where L is the crystallite size, K is a constant (0.9), λ is the X-ray wavelength, β is the FWHM (Full Width at Half Maximum) at 2θ x (π 180) and θ is the Bragg angle. From the calculation results using the Debye Scharrer equation, the crystallite sizes are obtained successively as shown in Table 1. From the table, it is evident that the crystallite size of the $Ni_{1-x}Cd_xFe_2O_4$ samples increases with the substitution of Cd^{2+} ions. This increase is attributed to the larger ionic radius of Cd^{2+}, which promotes the growth of larger crystallites.

Analysis by FTIR

FTIR analysis is conducted to identify the internal vibrational modes within the ferrite structure, which provide insights into the spatial positions of divalent and trivalent metal ions in the spinel lattice[30]. The FTIR analysis results of $NiFe_2O_4$ and $Ni_{1-x}Cd_xFe_2O_4$ (x = 0.1, 0.15, and 0.2) samples are presented in the FTIR spectrum shown in Figure 3.

Table 1. Crystal size of the sample $CdFe_2O_4$, $NiFe_2O_4$, and $Ni_{1-x}Cd_xFe_2O_4$

Samples	Crystal size (nm)
$CdFe_2O_4$	19
$NiFe_2O_4$	14.7
x = 0.1	8.6
x = 0.15	9.2
x = 0.2	9.5

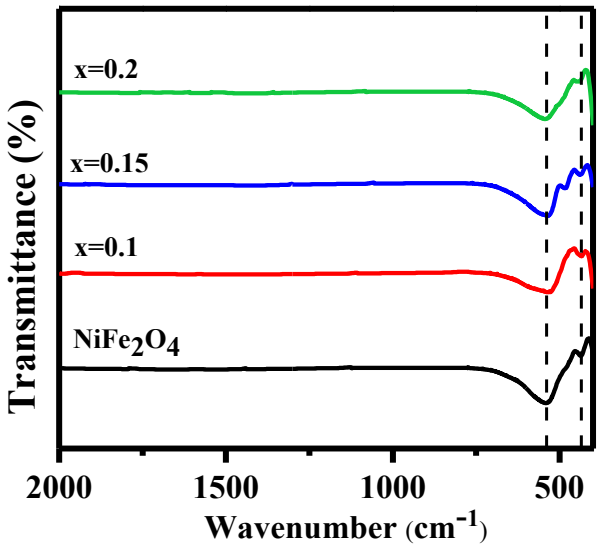

Figure 3. FTIR spectrum of $NiFe_2O_4$ and $Ni_{1-x}Cd_xFe_2O_4$

DOI: https://doi.org/ 10.25077/jrk.v16i2.855

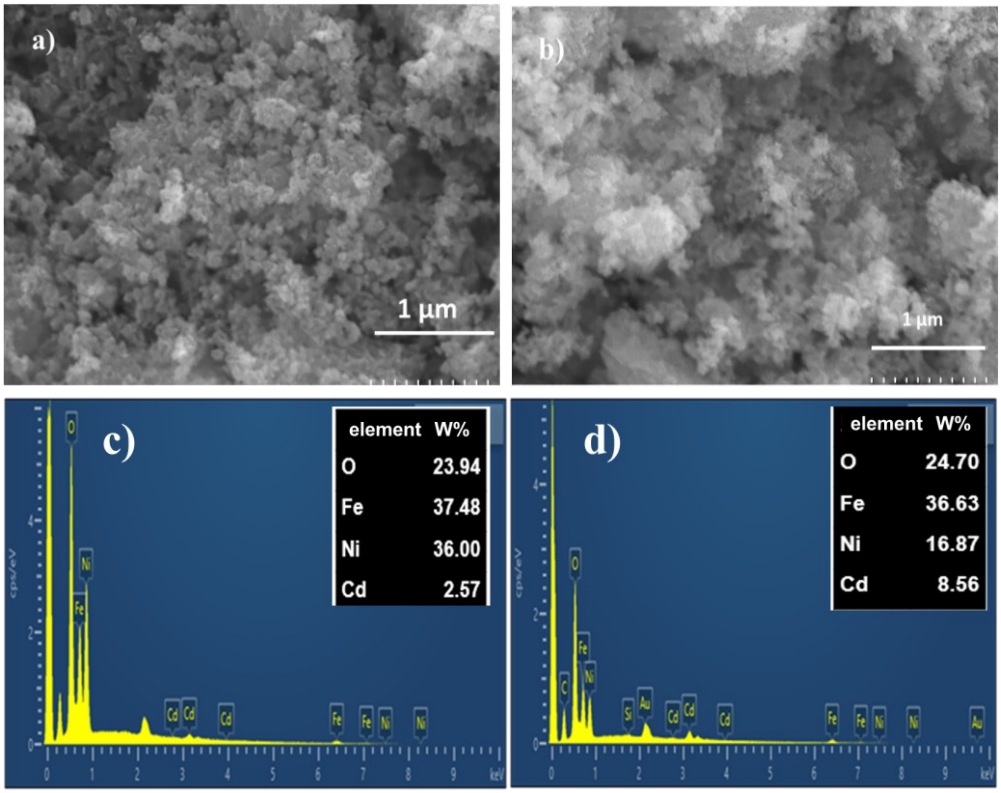

Figure 4. SEM images of $Ni_{1-x}Cd_xFe_2O_4$ with magnification of 30.000 [a) x= 0.1 and b) x=0.2] and EDS spectra of $Ni_{1-x}Cd_xFe_2O_4$ [c) x= 0.1 and d) x=0.2]

The absorption band observed at 440.86 cm^{-1} corresponds to the stretching vibrations of metal–oxygen bonds (Fe–O and Ni–O), which are associated with metal ions occupying the octahedral sites in the spinel ferrite structure. Absorption at wave number of 530.63 cm^{-1} shows the stretching vibration of metal-oxygen bonds (Fe-O) and (Cd-O) at the tetrahedral site[31]. For the $Ni_{1-x}Cd_xFe_2O_4$ sample, the vibration at wave number 530.86 cm-1 shifts to a smaller wave number with increasing amount of Cd^{2+} ions doped[7].

These findings indicate that a substitution occurs between Cd^{2+} and Ni^{2+} cations within the resulting $Ni_{1-x}Cd_xFe_2O_4$ spinel ferrite structure. The replacement of Ni^{2+} by the larger Cd^{2+} ions lead to an increase in the unit cell volume, which in turn results in the elongation of the Ni–O bonds in the octahedral sites. The elongation of these bonds reduces the Ni–O bond force constant, thereby causing a shift in the vibrational frequency toward lower wave numbers. This shift is consistent with Hooke's law, which states that the wave number is influenced by both the force constant and the mass of the vibrating atoms[32]. The absorption bands observed in the 300–700 cm^{-1} region correspond to the vibrational modes of M^{2+} and Fe^{3+} ion bonds within the spinel ferrite crystal lattice. The notable variations in the positions of these absorption bands are attributed to differences in interionic distances, as the cations are distributed between the tetrahedral and octahedral sites[33]. The absorption bands appearing at the octahedral and tetrahedral sites indicate the formation of spinel ferrite from $Ni_{1-x}Cd_xFe_2O_4$.

Analysis by SEM-EDS

The morphology, particle shape, and elemental composition of the synthesized materials were characterized using Scanning Electron Microscopy coupled with Energy Dispersive X-ray Spectroscopy (SEM-EDS). The samples analyzed correspond to compositions with x = 0.1 and x = 0.2. Surface morphology of the synthesized $Ni_{1-x}Cd_xFe_2O_4$ materials is presented in the SEM micrographs (Figure 4a and 4b),

while the elemental composition of each sample is shown in the corresponding EDS spectra (Figure 4c and 4d).

The SEM image of the $Ni_{1-x}Cd_xFe_2O_4$ sample with x = 0.1 (Figure 5a) reveals predominantly spherical or circular particles with minimal agglomeration. In contrast, the sample with x = 0.2 (Figure 5b) exhibits a similar particle shape but with a higher degree of agglomeration. Based on the SEM analysis, the sample with x = 0.1 appears to possess a more homogeneous particle distribution compared to the sample with x = 0.2. The increased concentration of Cd^{2+} ions in the sample is associated with enhanced particle agglomeration, which is likely attributed to the corresponding increase in magnetic interactions among particles. Furthermore, the autocombustion synthesis method employed in this study also plays a significant role in influencing particle growth during the formation of the magnetic nanoparticles[12].

The elemental composition of the $Ni_{1-x}Cd_xFe_2O_4$ compound was analyzed using Energy Dispersive X-ray Spectroscopy (EDS). The EDS spectra revealed that each synthesized material contained elements consistent with the expected composition, with no impurity detected. The identified elements in the samples included Fe, Ni, Cd, and O. The EDS data also showed a decrease in the concentration of Ni^{2+} ions accompanied by an increase in Cd^{2+} ions concentration, suggesting that a doping process occurred within the $Ni_{1-x}Cd_xFe_2O_4$ structure via a metal ion substitution mechanism.

Analysis by VSM

The magnetic properties of the samples were analyzed using VSM equipment. The hysteresis curve from the analysis results with VSM can be seen in Figure 5. From the shape of the hysteresis curve, it is exhibited that the $NiFe_2O_4$ sample is ferrimagnetic owing to its Mr value of 31.66 Tesla (T). For the $Ni_{1-x}Cd_xFe_2O_4$ sample (Figure 5b), for x=0.15 and 0.2 the remanent magnetization (Mr) and saturation magnetization (Ms) values increase with increasing amounts of Cd^{2+} ions dopants in the sample (Table 2), while the coercivity (Hc) value decreases with increasing concentrations of Cd^{2+} ions dopants in $Ni_{1-x}Cd_xFe_2O_4$. The variation in the magnetic properties of the sample is attributed to the difference in magnetic moments between nickel and cadmium cations [34]. An increase in Cd^{2+} ions content leads to enhanced magnetic properties, which is attributed to the larger particle size resulting from agglomeration. In contrast to the present study, Saha et al. reported that doping $NiFe_2O_4$ with Ag leads to a reduction in magnetic properties, attributed to a decrease in particle size [35]. The changes in magnetic characteristics of the synthesized ferrites are caused by several parameters. such as doping of metal cations, density, composition, porosity, morphology, homogeneity, and placement of cations in the crystal structure[2].

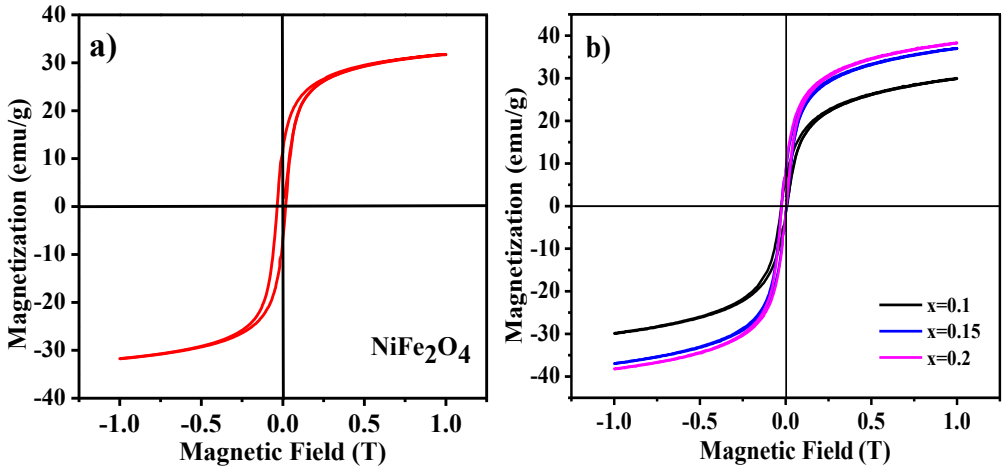

Figure 5. Hysteresis curve of (a) $NiFe_2O_4$ and (b) $Ni_{1-x}Cd_xFe_2O_4$ (x=0.1, 0.15, and 0.2)

 DOI: https://doi.org/ 10.25077/jrk.v16i2.855

Table 2. Magnetic properties of $Ni_{1-x}Cd_xFe_2O_4$ measured at room temperature

Sample	Ms (emu/g)	Mr (emu/g)	Hc (Oe)
$NiFe_2O_4$	31.663	11.259	344.92
x = 0.1	29.979	5.392	254.49
x = 0.15	36.965	6.921	230.28
x = 0.2	38.312	7.457	236.05

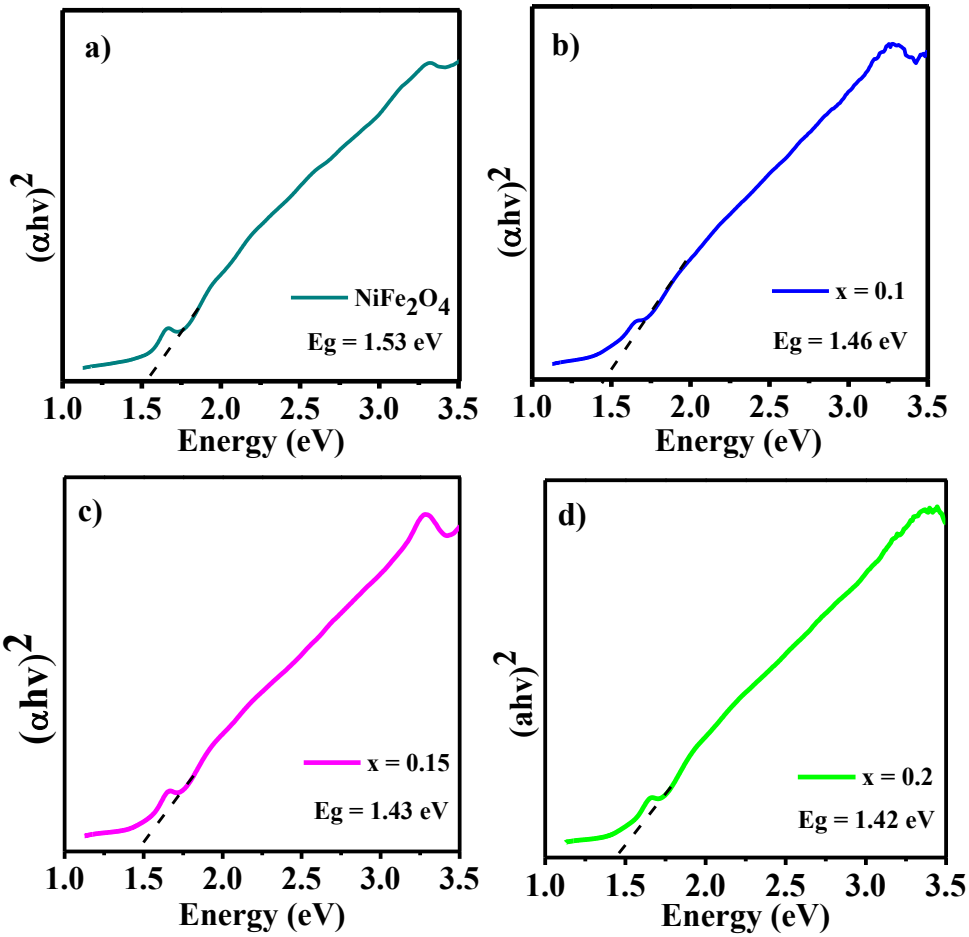

Figure 6. Band gap energy of $NiFe_2O_4$ a), $Ni_{1-x}Cd_xFe_2O_4$ b) x=0.1, c) x=0.15, and d) x= 0.2

Cd^{2+} ions are diamagnetic which tend to occupy the tetrahedral coordinated side. Due to the presence of 2 ions on the tetrahedral site (Ni^{2+} and Cd^{2+}) with large differences in their ionic radii, there is an increase in lattice distortion and a decrease in the overall magnetic moment of the crystal[10]. The change in the magnetic value of the sample indicates the formation of $Ni_{1-x}Cd_xFe_2O_4$ spinel ferrite and confirming that the sample exhibits ferrimagnetic behavior.

Analysis by DRS UV-Vis

The optical properties of $NiFe_2O_4$ and $Ni_{1-x}Cd_xFe_2O_4$ were analyzed using DRS UV-Vis equipment (Figure 6). The analysis of optical properties aims to see the ability of the material to absorb light in the visible light region. The band gap energy of the $NiFe_2O_4$ (Figure 6a) and $Ni_{1-x}Cd_xFe_2O_4$ samples (Figure 6b-d) were determined using the Tauc equation. According to Tauc, the absorption (α) of a material is related to its optical band gap energy (Eg) through the following equation[36]:

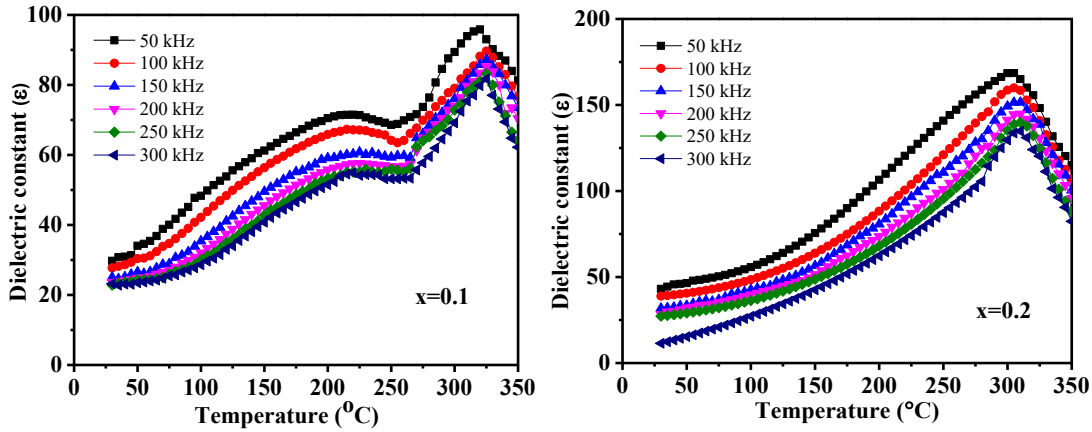

Figure 7. Dielectric constant of $Ni_{1-x}Cd_xFe_2O_4$ samples with x= 0.1 and 0.2

$$(\alpha h\nu)^2 = B(h\nu - Eg) \quad (2)$$

Where B is a constant that not depend on temperature, hν is the incoming photon energy and *Eg* is the gap energy.

To determine the value of the optical band gap, a plot was constructed between $(\alpha h\nu)^2$ and $h\nu$. From the graph, it can be seen that the energy gap value of $NiFe_2O_4$ is 1.53 eV, while for the $Ni_{1-x}Cd_xFe_2O_4$ sample, it is 1.46, 1.43, and 1.42 for x = 0.1, 0.15, and 0.2, respectively. From this value, it can be said that the sample is optical, which can absorb the visible light region. The decrease in the energy gap value of the $Ni_{1-x}Cd_xFe_2O_4$ sample occurred with increasing Cd doping concentration, which is estimated due to the overlap between the conduction band and the valence band. It is also can be attributed to the lattice defect, displacement of atom and grain boundary diffusion. The decrease in the band gap energy was also reported by Chandekar et al., 2023 who synthesized $NiFe_2O_4$ with Co doping. The decrease in the Eg value is associated with the quantum confinement effect, where the movement of electrons and holes is limited in a narrow space[37].

Analysis dielectric properties by LCR meter

The dielectric properties of materials are influenced by several factors including synthesis method, chemical composition, stoichiometry, porosity, ionic charge and cation distribution between tetrahedral and octahedral structures[38]. Dielectric properties are measured with an Inductance, Capacitance and Resistance (LCR) meter. The effect of Cd ion doping on the dielectric properties of $Ni_{1-x}Cd_xFe_2O_4$ samples was observed in the temperature range of 30 °C to 350 °C at various frequencies ranging from 50 kHz, 100 kHz, 150 kHz, 200 kHz, 250 kHz, to 300 kHz for all samples which reflects intrinsic factors of polarization and structural distortion. Figure 7 shows the dielectric properties of $Ni_{1-x}Cd_xFe_2O_4$ samples with different compositions and stoichiometries. The figure shows the relationship between dielectric constant (Ɛ) and temperature (T). The dielectric constant increases very slowly at temperature 30 °C up to a temperature of 50 °C and above this temperature the dielectric constant increases rapidly.

According to the Koop model, the dielectric constant is inversely proportional to the square root of the resistivity. Therefore, an increase in Ɛ with temperature is expected. The dielectric constant increases sharply at temperatures approaching the Curie temperature (Tc) of ferrite, where the material changes from a polarized phase to an unpolarized phase[39]. The dielectric constant increases with increasing Cd concentration in the ferrite compound $Ni_{1-x}Cd_xFe_2O_4$. The increase in the dielectric constant value is estimated due to the complex interactions between polarons, structural defects, and secondary phases in the material.

DOI: https://doi.org/ 10.25077/jrk.v16i2.855

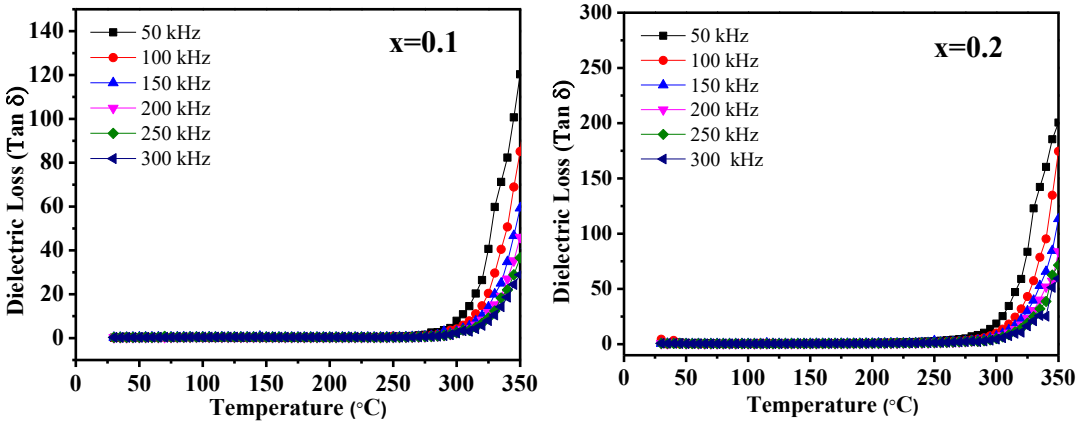

Figure 8. Dielektric loss of $Ni_{1-x}Cd_xFe_2O_4$ with x=0,1 and 0,2

Dielectric loss for $Ni_{1-x}Cd_xFe_2O_4$ samples (x=0; 0.1; and 0.2) was measured at frequencies from 50 kHz to 300 kHz. The relationship between dielectric loss and temperature shows two regions, namely the first zone from room temperature to about 250°C where Tanδ is almost constant, and the second zone from 30°C to above 250°C. Figure 8 exhibited that the dielectric loss is low at low temperatures for all Cd^{2+} doping concentrations, while at high temperatures the dielectric loss increases. Dielectric loss increases with increasing temperature above 250 °C due to the increase in electron hopping rate between Fe ions[29]. As a result, the maximum dielectric loss can be determined when the hopping frequency is almost the same as the frequency of the applied external electric field[21].

Conclusions

$Ni_{1-x}Cd_xFe_2O_4$ materials with different compositions (x = 0, 0.1, 0.15, and 0.2) have been synthesized by the autocombustion method using citric acid as fuel. Analysis with XRD instrument showed that $Ni_{1-x}Cd_xFe_2O_4$ has a cubic spinel structure with space group Fd-3m. FT-IR spectrum shows an absorption band at wave number 530.63 cm^{-1} for the octahedral site and a wave number 440.86 cm^{-1} for the tetrahedral site in the spinel ferrite structure, indicating the formation of spinel ferrite $Ni_{1-x}Cd_xFe_2O_4$. The sample contains Fe, Ni, Cd, and O elements as seen from EDS analysis. The energy band gap decreases with an increase in Cd^{2+} content x calculated by using UV- Visible data. The magnetic study displays an increase in saturation magnetization with decreasing coercivity with Cd doping. The measurement data using an LCR meter shows that with increasing Cd^{2+} doping, the dielectric properties of the sample increase. These fascinating characteristics of $Ni_{1-x}Cd_xFe_2O_4$ make it a valuable material to be used in magnetic recording, magnetic data storage, memory devices, and energy storage devices, etc.

Acknowledgments

We thank LPPM Andalas University for funding this research through the Penelitian Skripsi Sarjana (PSS) grant with contract number 225/UN16.19/PT.01.03/PSS/2024.

References

1. Tahir, W., Zeeshan, T., Waseem, S., Ali, M. D., Kayani, Z., Aftab, Z. e. H., Mehtab, S. M. T., *et al.*, Impact of silver substitution on the structural, magnetic, optical, and antibacterial properties of cobalt ferrite. *Sci. Rep.*, **13(1)**: 1–23 (2023).
2. Zahid, M., Khan, H. M., Zeewaqar Manzoor, M., Ejaz Ahmed, H., Akhter, T., Alshahrani, T., Imran, M., *et al.*, Optimization of structural, dielectric, and magnetic properties of nanocrystalline copper doped spinel ferrites. *Mater. Sci. Eng. B*, **(February)**: 116739 doi:10.1016/j.mseb.2023.116739
3. Sagadevan, S., Chowdhury, Z. Z. & Rafique, R. F., Preparation and

characterization of nickel ferrite nanoparticles via co-precipitation method. *Mater. Res.*, **21(2)**: 21–25 (2018).

4. S. G, D. & B, M., A comprehensive review on current trends in greener and sustainable synthesis of ferrite nanoparticles and their promising applications. *Results Eng.*, **21(December 2023)**: 101702 (2024).
5. -, M., Shofiah, S. & Suharyadi, E., Sintesis Nanopartikel Nickel Ferrite (NiFe2O4) dengan Metode Kopresipitasi dan Karakterisasi Sifat Kemagnetannya (Halaman 20 s.d. 25). *J. Fis. Indones.*, **19(56)**: 20–25 (2015).
6. Stiadi, Y., Wendari, T. P., Zilfa., Zulhadjri. & Rahmayeni., Tuning the structural, magnetic, and optical properties of ZnO/NiFe2O4 heterojunction photocatalyst for simultaneous photodegradation of Rhodamine B and Methylene Blue under natural sunlight. *Environmental Engineering Research*, **28(3)**: (2023).
7. Kardile, H. J., Somvanshi, S. B., Chavan, A. R., Pandit, A. A. & Jadhav, K. M., Effect of Cd2+ doping on structural, morphological, optical, magnetic and wettability properties of nickel ferrite thin films. *Optik (Stuttg).*, **207(August 2019)**: 164462 (2020).
8. Sun, L., Guo, J., Zhang, R., Cao, E., Zhang, Y., Hao, W. & Ju, L., Influence of Cu2+ doping on the structure, dielectric and magnetic properties of NiFe2O4 prepared by the sol-gel method. *J. Magn. Magn. Mater.*, **449**: 545–551 (2018).
9. Rajashekhar, K., Naik, J. L., Vinod, G., Kumar, K. M. & Sumathi, G., Structural and magnetic traits of Nd+3 doped copper rich nickel ferrite nanoparticles synthesized via citrate mediated sol-gel auto combustion route. *Ceram. Int.*, **50(20)**: 37607–37617 (2024).
10. Aakash., Nordblad, P., Rajendra Mohan. & Mukherjee, S., Structural, magnetic and hyperfine characterizations of nanocrystalline Zn-Cd doped nickel ferrites. *J. Magn. Magn. Mater.*, **441**: 710–717 (2017).
11. Süngü Mısırlıoğlu, B., Kahya, N. D. & Öztürk, Z., Enhanced dielectric properties of copper substituted nickel ferrite nanoparticles for energy storage applications. *J. Phys. Chem. Solids*, **193(May)**: (2024).
12. Devmunde, B. H., Bhalerao, P. S. & Solunke, M. B., Structural morphological and infrared properties of Cd2+ substitutes nickel ferrite particles. *J. Phys. Conf. Ser.*, **1644(1)**: (2020).
13. Bagade, A. V., Nagwade, P. A., Nagawade, A. V., Thopate, S. R. & Pund, S. N., A Review on Synthesis, Characterization and Applications of Cadmium Ferrite and its Doped Variants. *Orient. J. Chem.*, **38(1)**: 01–15 (2022).
14. Yaseneva, P., Bowker, M. & Hutchings, G., Structural and magnetic properties of Zn-substituted cobalt ferrites prepared by co-precipitation method. *Phys. Chem. Chem. Phys.*, **13(41)**: 18609–18614 (2011).
15. Salih, S. J. & Mahmood, W. M., Review on magnetic spinel ferrite (MFe2O4) nanoparticles: From synthesis to application. *Heliyon*, **9(6)**: e16601 (2023).
16. Suryawanshi, S. M., Chandekar, K. V., Badwaik, D. S. & Warhate, V. V., Structural , surface , magnetic , and dielectric properties of. **156(July)**: 111204 (2023).
17. Nandapure, A. I., Kondawar, S. B., Sawadh, P. S. & Nandapure, B. I., Effect of zinc substitution on magnetic and electrical properties of nanocrystalline nickel ferrite synthesized by refluxing method. *Phys. B Condens. Matter*, **407(7)**: 1104–1107 (2012).
18. Bharathi, K. K., Markandeyulu, G. & Ramana, C. V., Structural , Magnetic , Electrical , and Magnetoelectric Properties of Sm- and Ho-Substituted. 554–560 (2011).
19. Rahmayeni., Febrialita, R., Stiadi, Y., Putri, Y. E., Sofyan, N. & Zulhadjri., Simbang Darah (Iresine herbstii) extract mediated hydrothermal method in the synthesis of zinc ferrite spinel nanoparticles used for photocatalysis and antibacterial applications. *J. Environ. Chem. Eng.*, **9(2)**: (2021).

 DOI: https://doi.org/ 10.25077/jrk.v16i2.855

20. Sefthymaria, S., Nuryanto, R. & Taslimah, T., Pengaruh Variasi Chelating Agent terhadap Karakteristik Produk pada Sintesis Elektrolit Padat NaMn2-xMgxO4 dengan Metode Sol-Gel. *J. Kim. Sains dan Apl.*, **18(3)**: 79–84 (2015).
21. Hussain, A., Khalid, M., Chandio, A. D., Yasin, M., Abbas, N., Ashiq, M. G. B., Albalawi, H., *et al.*, Dielectrically modified Nd3+ doped (Ni–Mn) based spinel ferrite Ni0.5Mn0.5NdxFe2-xO4 nanoparticles for energy storage applications. *Phys. B Condens. Matter*, **666(May)**: 415135 (2023).
22. Porrawatkul, P., Nuengmatcha, P., Tangwatanakul, W. & Chanthai, S., Effect of Zn, Ni, and Mn doping ions on magnetic properties of MFe2O4 (M = Mn, Zn, and Ni) nanoparticles synthesized via sol–gel autocombustion using PVA/sago starch blend as a chelating agent. *J. Korean Ceram. Soc.*, **57(6)**: 676–683 (2020).
23. Rahmayeni, Arief, S., Stiadi, Y. & Rizal, R., *Synthesis of magnetic nanoparticles of TiO2-NiFe2O4: Characterization and Photocatalytic activity on Degradation of Rhodamine B*. *Indo. J. Chem*, **12(3)**: (2012).
24. Hedaoo, P. S., Badwaik, D. S., Suryawanshi, S. M. & Rewatkar, K. G., ScienceDirect Structural and Magnetic Studies of Zn Doped Nickel Nanoferrites Synthesize by Sol-gel Auto Combustion Method. *Mater. Today Proc.*, **15**: 416–423 (2019).
25. Silva, M. M. S., Raimundo, R. A., Ferreira, L. S., Macedo, D. A., Morales, M. A., Souza, C. P., Santos, A. G., *et al.*, Effects of morphology on the electrochemical performance of NiFe2O4 nanoparticles with battery-type behavior. *Int. J. Appl. Ceram. Technol.*, **19(4)**: 2016–2028 (2022).
26. Vasanthi, V., Shanmugavani, A., Sanjeeviraja, C. & Kalai Selvan, R., Microwave assisted combustion synthesis of CdFe 2O 4: Magnetic and electrical properties. *J. Magn. Magn. Mater.*, **324(13)**: 2100–2107 (2012).
27. De, M., Mukherjee, A. & Tewari, H. S., Characterization of cadmium substituted nickel ferrites prepared using auto-combustion technique. *Process. Appl. Ceram.*, **9(4)**: 193–197 (2015).
28. Jain, P., Shankar, S. & Thakur, O. P., Unveiling the structural, optical, electrical, and ferromagnetic properties of Ca2+ doped mixed spinel ferrites for switching field high-frequency device applications. *Ceram. Int.*, (2024). doi:10.1016/j.ceramint.2024.09.185
29. Mostafa, M. & Salem, B. I., Studying structural, molecular, morphological and electrical properties of Co0.2 Zn0.8 Fe2O4 doped with Cadmium. *Mater. Sci. Eng. B*, **286**: (2022).
30. Hu, J., Liu, X., Kan, X., Feng, S., Liu, C., Yang, Y. & Lv, Q., The changes in magnetic characteristics of the synthesized ferrites are caused by several parameters such as doping of metal cations, density, composition, porosity, morphology, homogeneity, and placement of cations in the crystal structure. *J. Alloys Compd.*, **828**: (2020).
31. Almessiere, M. A., Slimani, Y., Auwal, I. A., Shirsath, S. E., Gondal, M. A., Sertkol, M. & Baykal, A., Biosynthesis effect of Moringa oleifera leaf extract on structural and magnetic properties of Zn doped Ca-Mg nano-spinel ferrites. *Arab. J. Chem.*, **14(8)**: 103261 (2021).
32. Devi, C. S., Kumar, G. S. & Prasad, G., Control of ferroelectric phase transition in nano particulate NBT-BT based ceramics. *Mater. Sci. Eng. B*, **178(5)**: 283–292 (2013).
33. Ansari, M., Bigham, A., Hassanzadeh Tabrizi, S. A. & Abbastabar Ahangar, H., *Copper-substituted spinel Zn-Mg ferrite nanoparticles as potential heating agents for hyperthermia*. *Journal of the American Ceramic Society*, **101(8)**: (2018).
34. Parajuli, D. & Murali, N., Tailoring Structural and Magnetic Properties: Cd^{2+} and Cu^{2+} Co-Doped Ni-Zn Ferrite Nanoparticles via Sol-Gel Auto-Combustion. *South African J. Chem. Eng.*, (2024). doi:10.1016/j.sajce.2024.08.009
35. Saha, S., Routray, K. L., Hota, P., Dash, B., Yoshimura, S., Ratha, S. & Nayak, T. K., Structural, magnetic and dielectric

properties of green synthesized Ag doped NiFe2O4 spinel ferrite. *J. Mol. Struct.*, **1302**: (2024).

36. Rahmayeni, R., Oktavia, Y., Stiadi, Y., Arief, S. & Zulhadjri, Z., Spinel ferrite of MnFe2O4 synthesized in Piper betle Linn extract media and its application as photocatalysts and antibacterial. *J. Dispers. Sci. Technol.*, **42(3)**: 465–474 (2021).
37. Chandekar, K. V., Yadav, S. P., Chinke, S. & Shkir, M., Impact of Co-doped NiFe2O4 (CoxNi1−xFe2O4) nanostructures prepared by co-precipitation route on the structural, morphological, surface, and magnetic properties. *J. Alloys Compd.*, **966**: (2023).
38. Khatun, N., Osman Goni, M., Islam, M. S., Aftab Ali Shaikh, M., Uddin Farhad, S. F., Al-Mamun, M., Alam, M. S., *et al.*, Impact of lanthanum ions on structural, morphological, magnetic, optical and electrical properties of Cobalt-Zinc ferrites. *J. Magn. Magn. Mater.*, **614(December 2024)**: (2025).
39. Zhang, L. & Tang, Z. J., Polaron relaxation and variable-range-hopping conductivity in the giant-dielectric-constant material CaCu3Ti4O12. *Phys. Rev. B - Condens. Matter Mater. Phys.*, **70(17)**: 1–6 (2004).

 DOI: https://doi.org/ 10.25077/jrk.v16i2.855